JACS
JOURNAL OF THE AMERICAN CHEMICAL SOCIETY

COMMUNICATION

pubs.acs.org/JACS

One-Pot Synthesis of $Cu_{1.94}S$−CdS and $Cu_{1.94}S$−$Zn_xCd_{1-x}S$ Nanodisk Heterostructures

Michelle D. Regulacio,[†] Chen Ye,[†,‡] Suo Hon Lim,[†] Michel Bosman,[†] Lakshminarayana Polavarapu,[‡] Wei Ling Koh,[†] Jie Zhang,[†] Qing-Hua Xu,[*,‡] and Ming-Yong Han[*,†,§]

[†]Institute of Materials Research and Engineering, Agency for Science, Technology and Research, 3 Research Link, Singapore 117602

[‡]Department of Chemistry, National University of Singapore, 3 Science Drive 3, Singapore 117543

[§]Division of Bioengineering, National University of Singapore, 9 Engineering Drive 1, Singapore 117576

Supporting Information

ABSTRACT: Nanodisk heterostructures consisting of monoclinic $Cu_{1.94}S$ and wurtzite CdS have been colloidally synthesized for the first time. Initially, hexagonal-shaped nanodisks of $Cu_{1.94}S$ were produced upon thermolysis of a copper complex in a solvent mixture of HDA and TOA at 250 °C. Rapid addition of Cd precursor to the reaction mixture resulted in the partial conversion of $Cu_{1.94}S$ into CdS, yielding $Cu_{1.94}S$−CdS nanoheterostructures. The original morphology of the $Cu_{1.94}S$ nanodisks was conserved during the transformation. When Zn precursor was added together with the Cd precursor, $Cu_{1.94}S$−$Zn_xCd_{1-x}S$ nanodisks were generated. These two-component nanostructures are potentially useful in the fabrication of heterojunction solar cells.

Binary copper sulfides (Cu_xS, where $x = 1-2$) are known to exist in a number of stable and metastable phases with stoichiometries ranging from Cu_2S (chalcocite) to CuS (covellite).[1] Because of the copper vacancies within their lattice, these compounds are excellent p-type semiconducting materials displaying great promise as light-absorbing component in solar cell devices. The use of p-type Cu_2S coupled to n-type CdS in the fabrication of cost-efficient thin-film heterojunction solar cells has been widely investigated in the past and power conversion efficiencies (PCEs) of up to 9% have been reported.[2] In recent years, the use of nanomaterials in photovoltaic device fabrication is being explored in the hope of significantly enhancing the performance and reducing the manufacturing cost of solar cells. For example, nanocrystal-based heterojunction solar cells have been fabricated by creating thin films that consist of separate layers of p-type and n-type semiconductor nanocrystals.[3] One drawback in the design of this device is the insufficient contact between the two semiconductor components that form the heterojunction due to the layer of organic surfactants capping the nanocrystals. In this communication, we report the solution-phase synthesis of nanoscale heterojunctions consisting of p-type $Cu_{1.94}S$ and n-type semiconductors such as CdS and $Zn_xCd_{1-x}S$. In these nanoheterostructures, the two semiconductor components that make up the heterojunction are in direct contact with each other and are contained within a single nanocrystal. This design promotes the spatial separation of carriers, which is necessary in the development of a highly efficient solar cell device.

Over the past decade, several studies on the synthesis of nanocrystalline Cu_xS have been published, most of which reports on stoichiometric Cu_2S.[4] Copper dithiocarbamate complexes have been previously utilized as molecular precursors to produce spherical $Cu_{1.8}S$ (digenite) nanocrystals[5] and ultrathin nanowires of β-Cu_2S (high-temperature chalcocite).[6] Herein, we demonstrate the use of $Cu(S_2CNEt_2)_2$ in the colloidal synthesis of $Cu_{1.94}S$ (djurleite) nanodisks and their nanoscale heterostructures.

Figure 1a shows the X-ray diffraction (XRD) pattern of the nanocrystals obtained by swiftly injecting a solution of $Cu(S_2CNEt_2)_2$ to a solvent mixture consisting of hexadecanethiol (HDT) and trioctylamine (TOA) at 250 °C (see Supporting Information for experimental details). All the diffraction peaks can be indexed to monoclinic $Cu_{1.94}S$ (JCPDS no. 34-0660). The representative transmission electron microscopy (TEM) image displayed in Figure 1c (also see Figure S1a in Supporting Information) reveals that the product consists of hexagonal-shaped disks with an average diameter of 41.7 ± 3.3 nm and thickness of 15.9 ± 1.0 nm (measured from a population of 135 nanodisks). Most of the nanodisks prefer to orient perpendicular to the substrate and self-assemble into strands of stacked disks (as shown in the circled area). The use of other solvents/solvent mixtures was investigated, and the phase and morphology of the resulting nanocrystals are tabulated in Table S1 in Supporting Information (TEM images and XRD patterns are shown in Figures S1 and S2). The formation of $Cu_{1.94}S$ is favored when the copper dithiocarbamate complex is decomposed in the presence of thiols. Aside from their ability to act as capping ligands, thiols also provide a sulfur-rich environment and may function as an additional sulfur source inducing the formation of a nonstoichiometric Cu_xS phase with higher sulfur content than stoichiometric Cu_2S.

Rapid addition of $Cd(S_2CNEt_2)_2$ a few minutes after the injection of the $Cu_{1.94}S$ precursor has led to the formation of colloidal heterostructured nanocrystals which, based on the XRD pattern (Figure 1b), are composed of monoclinic $Cu_{1.94}S$ and wurtzite CdS (JCPDS no. 77-2306). A partial cation-exchange reaction is believed to occur because the hexagonal shape of the

Received: October 8, 2010
Published: January 31, 2011

dx.doi.org/10.1021/ja1090589 | J. Am. Chem. Soc. 2011, 133, 2052–2055

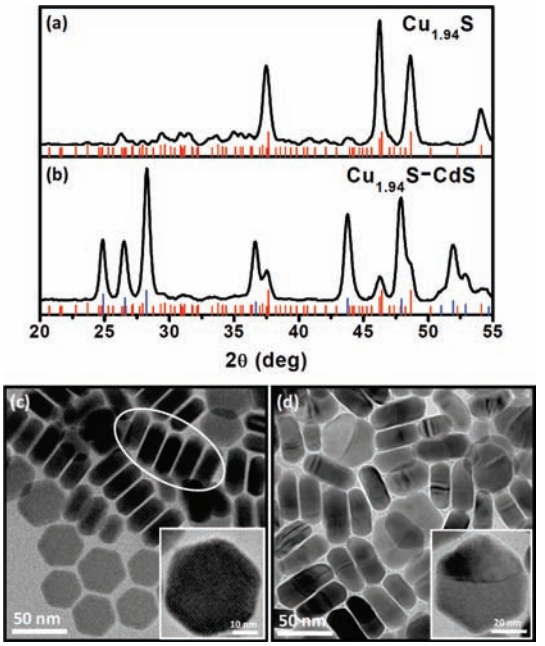

Figure 1. XRD patterns of the as-obtained (a) $Cu_{1.94}S$ and (b) $Cu_{1.94}S$−CdS nanodisks. Red and blue lines are from standard JCPDS file of monoclinic $Cu_{1.94}S$ [34-0660] and wurtzite CdS [77-2306], respectively. TEM images of (c) $Cu_{1.94}S$ and (d) $Cu_{1.94}S$−CdS nanodisks. Circled area in (c) shows self-assembly of nanodisks that are oriented perpendicular to the substrate. The insets in (c) and (d) display the hexagonal morphology of representative nanodisks.

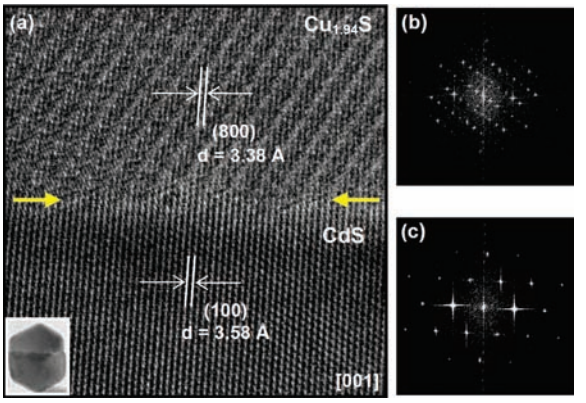

Figure 2. (a) HRTEM image of a portion of a $Cu_{1.94}S$−CdS nanodisk. Yellow arrows are used to highlight the epitaxial interface. The inset shows the low-resolution TEM image of the entire nanodisk. (b−c) FFT patterns of the top and bottom regions in (a).

initially formed $Cu_{1.94}S$ nanodisks has been preserved as seen in the TEM images in Figures 1d and S3. On the basis of the study of Alivisatos' group, the anionic framework of ionic nanocrystals is found to be conserved during cation-exchange reactions, and this enables the preservation of the original morphology of the reactant nanocrystals.[7]

The high-resolution TEM (HRTEM) image in Figure 2a clearly shows an interface between two different materials within a single nanodisk (interface highlighted by yellow arrows). The fast Fourier transform (FFT) patterns (Figures 2b−c) that are obtained from two sections of the disk, one on each side of the interface, are noticeably dissimilar, confirming the presence of

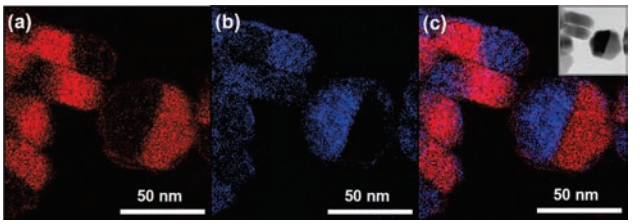

Figure 3. EFTEM images of $Cu_{1.94}S$−CdS nanodisks showing the (a) Cu and (b) Cd elemental maps. The composite EFTEM image is displayed in (c). Cu-containing regions are coded red, whereas Cd-containing segments are coded blue. The inset in (c) shows the corresponding bright-field TEM image.

two distinct phases within the nanodisk. Analysis of the lattice spacing reveals that the (800) planes of $Cu_{1.94}S$ (d = 3.38 Å) are coincident with the (100) planes of CdS (d = 3.58 Å). Figure S4 displays the high-angle annular dark-field scanning TEM (HAADF-STEM) image of a representative nanodisk and the energy-dispersive X-ray (EDX) spectra measured from two different regions of the disk. The EDX spectra show peaks attributed to the presence of Cu and S in one side of the phase boundary, and the presence of Cd and S in the other side. This further supports the formation of a nanoheterostructure that is composed of two different sulfide materials. Energy-filtered TEM (EFTEM) was used to obtain elemental distribution maps of Cu and Cd in the two-component nanostructures. The red regions in the images shown in Figure 3 are the Cu-containing portions of the nanodisks, whereas the blue regions are the Cd-containing segments. We have observed that in majority of the as-synthesized nanodisks, the $Cu_{1.94}S$ and CdS portions are nearly equal in size. We are currently working on tuning the relative size of the $Cu_{1.94}S$ and CdS regions within the nanocrystals by varying the synthetic parameters that affect the extent of the cation-exchange reaction.

Employing a different Cd^{2+} source ($Cd(CH_3COO)_2$) in place of $Cd(S_2CNEt_2)_2$ has also resulted in the formation of hexagonal-shaped $Cu_{1.94}S$−CdS nanodisks (TEM images and XRD pattern are shown in Figure S5). This is a further indication that our nanodisk heterostructures are generated through partial Cd^{2+} cation exchange. The strong structural similarity (i.e., nearly identical hexagonal close-packed sulfur lattice) of CdS and most of the binary Cu_xS phases has allowed one to be transformed to another by a simple cation exchange. In a report by Cook and co-workers, bulk crystals of CdS can be converted to Cu_xS (x = 2, 1.96, and 1.96 > x > 1.8) by cation exchange when dipped in a solution containing CuCl.[8] More recently, the selectivity for Cu^+ cation exchange to occur at different facets of CdS nanorods has been demonstrated.[7b] The hexagonal-shaped disk morphology of our $Cu_{1.94}S$ nanocrystals exposes many different crystallographic facets. Cation exchange with Cd^{2+} will preferentially begin at the facet that will give the lowest interface formation energy (i.e., most stable interface). Unfortunately, we have observed that electron beam causes damages to our nanocrystals, and this has prevented conducting a more detailed HRTEM analysis of the surface facets and the interfaces formed in our nanoscale heterostructures.

When $Zn(S_2CNEt_2)_2$ is injected together with the Cd precursor into a hot solution of $Cu_{1.94}S$ nanodisks, nanoheterostructures consisting of $Cu_{1.94}S$ and ternary-alloyed $Zn_xCd_{1-x}S$ are produced (TEM images are displayed in Figure S6). The presence of both $Cu_{1.94}S$ and $Zn_xCd_{1-x}S$ is evidenced by the two

dx.doi.org/10.1021/ja1090589 |J. Am. Chem. Soc. 2011, 133, 2052–2055

sets of diffraction peaks in the XRD patterns shown in Figure S7. None of the peaks can be indexed to ZnS, which rules out the presence of a ZnS region within the nanodisks or the occurrence of homogeneous nucleation of ZnS nanocrystals. The diffraction peaks that are attributed to the presence of wurtzite $Zn_xCd_{1-x}S$ systematically shift toward higher 2θ values with increasing Zn content. This is indicative of the decrease in lattice parameters due to the smaller ionic radius of Zn^{2+} relative to Cd^{2+}. Previous work in our laboratory has shown that the lattice constant c of alloyed $Zn_xCd_{1-x}S$ nanocrystals varies linearly with composition in accordance to Vegard's law.[9] We have calculated the value of c for the $Zn_xCd_{1-x}S$ region in our nanodisks from the diffraction peaks in Figure S7. The actual alloy composition determined using the Vegard's law plot (Figure S8) is consistent with the Zn:Cd molar ratio used in the synthesis.

To the best of our knowledge, this is the first time that two-component nanostructures with hexagonal disk morphology have been prepared via a facile one-pot colloidal synthetic approach. Nanocrystal heterostructures that are reported in the literature are mostly of the core−shell type, which are often created from spherical nanocrystals. However, this type of nanoheterostructures cannot be used for applications that require dual-surface functionality (i.e., surface exposure of the two components that have different functionalities). Colloidal nanocrystals having anisotropic shapes are of great interest because the variation in surface facet reactivities enables the preparation of nanoheterostructures with complex morphologies, thus providing a means for nanocrystal engineering. Because of the selectivity for cation exchange to preferentially occur at different facets, partial Cd^{2+} cation exchange in our multifaceted $Cu_{1.94}S$ nanodisks enabled the formation of a dual-surface nanoscale p−n junction, with p-type $Cu_{1.94}S$ on one side and n-type CdS on the other. This design is expected to promote exciton dissociation due to the built-in electric field created by the p−n junction. In addition, the Cu_xS−CdS heterojunction exhibits a type II band alignment, which also provides a driving force for charge separation.[10] These nanoscale heterostructures are thus potentially useful in solar cell technology, where improved carrier separation efficiency is desirable.

The optical absorption spectra (Figure 4) of the $Cu_{1.94}S$ and $Cu_{1.94}S$−CdS nanodisks show significant absorbance across the solar spectrum. The weak NIR absorption seen in both spectra is derived from the intraband absorbance of free carriers, more specifically of holes associated with the presence of Cu vacancies in nonstoichiometric $Cu_{1.94}S$.[11] The shoulder at ∼490 nm (2.53 eV) in the absorption spectrum of the $Cu_{1.94}S$−CdS nanodisks is attributed to the excitonic absorption of CdS (bulk band gap = 2.5 eV). For comparison, a typical absorption spectrum of CdS nanorods is shown in Figure S9. The presence of the absorption features of both $Cu_{1.94}S$ and CdS in the spectrum of the $Cu_{1.94}S$−CdS nanodisks suggests that the photon can be absorbed by either of the two components.

The direct band gap, E_g, of Cu_xS is stoichiometry-dependent, with E_g increasing as x decreases due to the narrowing of the Cu d band (valence band) as well as the Moss−Burstein effect (i.e., lowering of the Fermi level into the valence band).[11] From the plot of the square of the absorbance vs the photon energy (Figure S10), we have obtained 2.29 eV as the optical E_g of our $Cu_{1.94}S$ nanodisks. This is largely blue-shifted from the bulk value of 1.8 eV that has been reported for djurleite thin films.[12] The band gap shift is a result of the quantum confinement effect, which has also been observed in nanocrystals of other binary copper sulfides.[4d] The photoluminescence (PL) spectrum (Figure 4 inset) of the $Cu_{1.94}S$ nanodisks shows luminescence bands peaking at 440 and 465 nm, and a shoulder at ∼490 nm. Interestingly, the PL spectrum of the $Cu_{1.94}S$−CdS nanodisks reveals that the $Cu_{1.94}S$ emission is considerably quenched in the nanoheterostructures. Moreover, the intense visible excitonic emission typically exhibited by CdS is not seen in the PL spectrum of the heterostructured nanodisks. These observations strongly imply that the photogenerated electrons and holes are spatially well separated in the nanodisk heterostructures, disfavoring recombination via radiative exciton emission. An investigation of the carrier dynamics using ultrafast laser spectroscopy (see Supporting Information, Figure S11) reveals that the carrier separation is based on a donor−acceptor charge transfer. An ultrafast electron transfer from $Cu_{1.94}S$ to CdS with a charge transfer rate of 0.80 ps is observed.

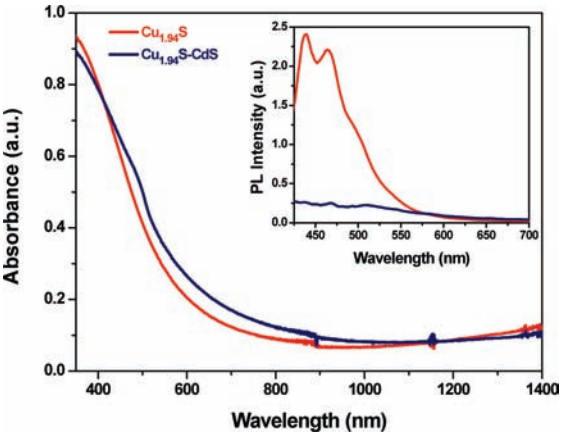

Figure 4. Absorption and PL (inset) spectra of $Cu_{1.94}S$ (red) and $Cu_{1.94}S$−CdS (blue) nanodisks. PL spectra were taken at 400-nm excitation.

In summary, hexagonal-shaped nanodisks of nonstoichiometric $Cu_{1.94}S$ have been colloidally prepared through thermal decomposition of a copper dithiocarbamate precursor in the presence of long-chain thiols. Partial cation exchange enabled the synthesis of heterostructured nanodisks, wherein p-type $Cu_{1.94}S$ and n-type semiconductors such as CdS and $Zn_xCd_{1-x}S$ are contained within a single nanodisk. This nanostructure design is effective in spatially separating the photogenerated carriers as evidenced by photoluminescence and ultrafast spectroscopy. The utility of these nanoscale heterostructures as the active component in heterojunction solar cells will be further evaluated in future work.

■ ASSOCIATED CONTENT

Supporting Information. Experimental procedures, TEM images, XRD patterns, EDX spectra, Vegard's law plot, absorption spectra, and discussion of carrier dynamics. This material is available free of charge via the Internet at http://pubs.acs.org.

■ AUTHOR INFORMATION

Corresponding Author
chmxqh@nus.edu.sg; my-han@imre.a-star.edu.sg

■ REFERENCES

(1) Chakrabarti, D. J.; Laughlin, D. E. *Bull. Alloy Phase Diagrams* **1983**, *4*, 254–271.

(2) (a) Rothwarf, A.; Barnett, A. M. *IEEE Trans. Electron Devices* **1977**, *24*, 381–387. (b) Devaney, W. E.; Barnett, A. M.; Storti, G. M.; Meakin, J. D. *IEEE Trans. Electron Devices* **1979**, *26*, 205–210. (c) Bragagnolo, J. A.; Barnett, A. M.; Phillips, J. E.; Hall, R. B.; Rothwarf, A.; Meakin, J. D. *IEEE Trans. Electron Devices* **1980**, *27*, 645–650.

(3) (a) Stavrinadis, A.; Smith, J. M.; Cattley, C. A.; Cook, A. G.; Grant, P. S.; Watt, A. A. R. *Nanotechnology* **2010**, *21*, 185202. (b) Wu, Y.; Wadia, C.; Ma, W.; Sadtler, B.; Alivisatos, A. P. *Nano Lett.* **2008**, *8*, 2551–2555.

(4) (a) Li, X.; Shen, H.; Niu, J.; Li, S.; Zhang, Y.; Wang, H.; Li, L. S. *J. Am. Chem. Soc.* **2010**, *132*, 12778–12779. (b) Wang, Y.; Hu, Y.; Zhang, Q.; Ge, J.; Lu, Z.; Hou, Y.; Yin, Y. *Inorg. Chem.* **2010**, *49*, 6601–6608. (c) Li, S.; Wang, H. Z.; Xu, W. W.; Si, H. L.; Tao, X. J.; Lou, S.; Du, Z.; Li, L. S. *J. Colloid Interface Sci.* **2009**, *330*, 483–487. (d) Zhao, Y.; Pan, H.; Lou, Y.; Qiu, X.; Zhu, J. J.; Burda, C. *J. Am. Chem. Soc.* **2009**, *131*, 4253–4261. (e) Lim, W. P.; Wong, C. T.; Ang, S. L.; Low, H. Y.; Chin, W. S. *Chem. Mater.* **2006**, *18*, 6170–6177. (f) Ghezelbash, A.; Korgel, B. A. *Langmuir* **2005**, *21*, 9451–9456. (g) Sigman, M. B. J.; Ghezelbash, A.; Hanrath, T.; Saunders, A. E.; Lee, F.; Korgel, B. A. *J. Am. Chem. Soc.* **2003**, *125*, 16050–16057.

(5) Lou, Y.; Samia, A. C. S.; Cowen, J.; Banger, K.; Chen, X.; Lee, H.; Burda, C. *Phys. Chem. Chem. Phys.* **2003**, *5*, 1091–1095.

(6) Liu, Z.; Xu, D.; Liang, J.; Shen, J.; Zhang, S.; Qian, Y. *J. Phys. Chem. B* **2005**, *109*, 10699–10704.

(7) (a) Jain, P. K.; Amirav, L.; Aloni, S.; Alivisatos, A. P. *J. Am. Chem. Soc.* **2010**, *132*, 9997–9999. (b) Sadtler, B.; Demchenko, D. O.; Zheng, H.; Hughes, S. M.; Merkle, M. G.; Dahmen, U.; Wang, L.-W.; Alivisatos, A. P. *J. Am. Chem. Soc.* **2009**, *131*, 5285–5293. (c) Luther, J. M.; Zheng, H.; Sadtler, B.; Alivisatos, A. P. *J. Am. Chem. Soc.* **2009**, *131*, 16851–16857.

(8) Cook, W. R.; Shiozawa, L.; Augustine, F. *J. Appl. Phys.* **1970**, *41*, 3058–3063.

(9) (a) Zhong, X.; Feng, Y.; Knoll, W.; Han, M. Y. *J. Am. Chem. Soc.* **2003**, *125*, 13559–13563. (b) Regulacio, M. D.; Han, M. Y. *Acc. Chem. Res.* **2010**, *43*, 621–630.

(10) Li, X.; Shen, H.; Li, S.; Niu, J. Z.; Wang, H.; Li, L. S. *J. Mater. Chem.* **2010**, *20*, 923–928.

(11) Lukashev, P.; Lambrecht, W. R. L. *Phys. Rev. B.* **2007**, *76*, 195202.

(12) Rastogi, A. C.; Salkalachen, S. *Thin Solid Films* **1982**, *97*, 191–199.